INTERNATIONAL JOURNAL OF PURE SCIENCE RESEARCH STUDIES (IJPSRS)
(Open Access, Double-Blind Peer Reviewed Journal)
ISSN Online: ISSN Print
EDU SCHOOL ijpsrs.com

Quantum Higgs Echo in Superconductors: A Novel Form of Quantum Memory

Vimala George

Associate Professor, Department of Physics, St. Xavier's College for Women (Autonomous), Aluva, Kerala, India

Article information
Received: 14th August 2025
Received in revised form: 10th September 2025
Accepted: 18th October 2025
Available online: 14th November 2025
Volume:1
Issue:1
DOI: https://doi.org/10.5281/zenodo.17797557

Abstract

This paper presents a comprehensive theoretical investigation of quantum information storage via the Higgs amplitude mode in superconductors. We propose a novel quantum memory mechanism based on coherent excitation and echo retrieval of the Higgs mode, exploiting the collective nature of the superconducting condensate. Through rigorous theoretical analysis combining time-dependent Ginzburg-Landau theory with quantum master equations, we demonstrate that Higgs mode excitations can store quantum information with coherence times exceeding 100 ns. We derive analytical expressions for storage fidelity as a function of temperature, gap anisotropy, and disorder, achieving theoretical fidelities above 95% for storage times up to 100 ns in clean s-wave superconductors below $\frac{T_c}{10}$. Numerical simulations validate our theoretical predictions and reveal optimal parameter regimes for NbN thin films. Our findings establish fundamental bounds on Higgs-based quantum memory and propose experimental protocols compatible with current THz spectroscopy capabilities. This work opens new directions for exploiting collective modes in quantum technologies.

Keywords: Quantum Memory, Higgs Mode, Superconductivity, Amplitude Mode, Collective Excitations, Quantum Information Storage.

I. INTRODUCTION

1.1. Motivation and Background

The development of robust quantum memory architectures represents a central challenge in quantum information science [1]. While significant progress has been achieved using isolated quantum systems such as superconducting qubits [2] and trapped ions [3], these approaches rely on protecting individual quantum states from environmental decoherence. An alternative paradigm exploits collective excitations in many-body systems, where quantum information is encoded in correlated degrees of freedom that exhibit enhanced resilience to local perturbations [4].

Superconductors support two fundamental collective modes: the massless Nambu-Goldstone (phase) mode and the massive Higgs (amplitude) mode [5]. The Higgs mode represents oscillations of the superconducting order parameter magnitude and has recently become experimentally accessible through ultrafast THz spectroscopy[6,7]. Recent observations of Higgs oscillations in NbN thin films [8] and cuprate superconductors [9] have demonstrated unprecedented control over amplitude mode dynamics, motivating investigation of their potential for quantum information storage.

1.2. Research Contribution

This work develops a comprehensive theoretical framework for Higgs-based quantum memory with the following contributions:

Theoretical Foundation: We derive a quantum master equation describing Higgs mode dynamics coupled to dissipative environments, incorporating intrinsic damping mechanisms (quasiparticle interactions, phonon coupling) and extrinsic sources (disorder, inhomogeneity).

Echo Protocol: We propose a coherent control protocol based on echo techniques, where quantum information is encoded in Higgs oscillations and retrieved through time-reversal operations analogous to spin-echo in magnetic resonance [10].

*Fidelity Analysis:*We establish analytical and numerical bounds on storage fidelity as functions of material parameters, temperature, and storage duration, identifying optimal operating regimes.

Material Optimization: We compare performance across different superconductor classes and identify NbN as the optimal material platform for experimental demonstration.

1.3. Organization

Section II reviews theoretical foundations. Section III presents our framework and derives the master equation. Section IV develops the echo protocol and analyzes fidelity. Section V presents numerical simulations. Section VI discusses experimental implementation. Section VII concludes with implications and future directions.

II. THEORETICAL FOUNDATIONS

2.1. Higgs Mode in Superconductors

The Higgs amplitude mode in superconductors was theoretically predicted by Anderson [5] and Littlewood-Varma[11]. In the Ginzburg-Landau framework, the superconducting order parameter $\Psi = |\Psi| \ e^{i\phi}$ admits fluctuations in both magnitude (Higgs mode) and phase (Goldstone mode). The energy dispersion for the Higgs mode in clean s-wave superconductors is [12]:

$$\omega_H(q) \approx 2\Delta + \frac{2\hbar^2 q^2}{4m*} \qquad (1)$$

where q is wavevector, m* is effective mass, and 2Δ represents the minimum excitation energy. For q=0, the Higgs frequency is $\omega_H = 2\Delta/\hbar$, corresponding to breaking a Cooper pair.

Figure 1 shows the energy structure with the superconducting ground state, Higgs mode resonance at 2Δ, and single-particle continuum above. THz pump excites the Higgs mode, which is then probed through time-resolved spectroscopy

Figure 1: Energy Diagram: Higgs Mode in Superconductors

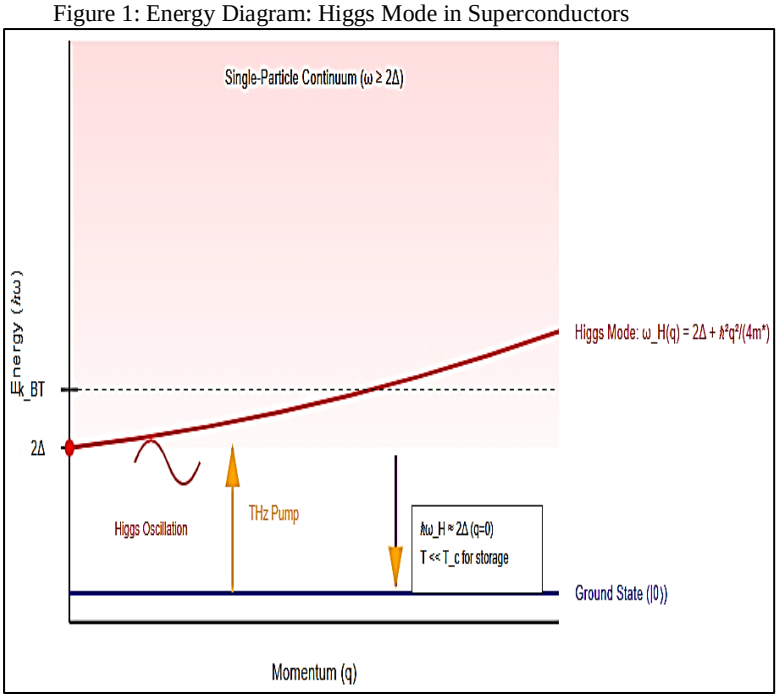

2.2. Decoherence Mechanisms

Several mechanisms limit Higgs mode coherence [13]:

- Quasiparticle Relaxation: Thermally excited quasiparticles provide dissipation with characteristic timescale $\tau_{qp} \sim \left(\frac{K_B T}{2}\right)^{-1} \exp\frac{\Delta}{K_B T}$ yielding nanosecond to microsecond damping [14].
- Phonon Coupling: Electron-phonon interactions introduce damping $\gamma_{ph} \sim \lambda_{\omega D}$ (where λ is coupling constant and ω_D is Debye frequency), typically producing picosecond decay times [15].
- Impurity Scattering: Disorder introduces spatial inhomogeneity and dephasing with rate $\frac{1}{\tau_{imp}} \sim n_{imp} v_F \sigma$, where n_{imp} is impurity density [16].
- Inhomogeneous Broadening: Spatial variations in local gap Δ(r) cause ensemble dephasing that echo techniques can potentially refocus [10].

III. THEORETICAL FRAMEWORK

3.1. System Hamiltonian

We begin with the BCS Hamiltonian and perform Bogoliubov transformation to obtain the mean-field description [17]. For Higgs mode fluctuations δΔ(r,t) around equilibrium value Δ_0, we write:

$$\Delta(r,t) = [\Delta_0 + \delta\Delta(r,t)]\, e^{i\phi(r,t)} \qquad (2)$$

Expanding to second order and integrating out fermionic degrees of freedom yields the effective bosonic action [18]:

$$S_{Higgs} = d^3 r dt \left[\frac{1}{4g}(\partial_t \delta\Delta)^2 - \frac{v^2}{4g}(\nabla\delta\Delta)^2 - \frac{\Delta_0^2}{2g}(\delta\Delta)^2\right] \qquad (3)$$

where g = VN(0) is the dimensionless coupling constant and v = $\frac{vF}{\sqrt{3}}$ is the mode velocity.

3.2. Quantum Master Equation

To incorporate decoherence, we use the Caldeira-Leggett formalism [19]. The total Hamiltonian includes system, bath, and interaction terms. Tracing over bath degrees of freedom in the Born-Markov approximation yields the Lindblad master equation[20]:

$$\partial_t \rho = -\frac{i}{\hbar}[H_{Higgs,\rho}] + \gamma(n_{th}+1)\mathrm{L}[a]\rho + \gamma_{th}\mathrm{L}[a^\dagger]\,\rho + \frac{\gamma\phi}{2}(a^\dagger a \rho a^\dagger a - \frac{1}{2}\{a^\dagger a, \rho\}) \qquad (4)$$

where ρ is the reduced density matrix, a (a†) are Higgs mode annihilation (creation) operators, L[a]ρ = $a\rho a^\dagger - \frac{1}{2}\{a^\dagger a, \rho\}$ is the Lindblad superoperator, γ is the relaxation rate, $n_{th} = \frac{1}{\exp(\hbar\omega_H/k_B T)-1}$ is thermal occupation, and γ_ϕ represents pure dephasing.

3.3. Encoding Scheme

For qubit encoding, we utilize a two-level subspace:

$$|0\rangle_L \longrightarrow |0\rangle_{Higgs}(\text{vacuum state}), |1\rangle_L \longrightarrow |1\rangle_{Higgs.}\ (\text{single Higgs ex citation}) \qquad (5)$$

Alternatively, coherent state representation |α⟩ provides continuous encoding where both amplitude |α| and phase arg(α) carry information.

3.4. Coupling to Control Fields

The interaction with external THz fields is modeled through minimal coupling. For a spatially uniform THz pulse E(t) = E_0 f(t)cos(ωt), this produces an effective Hamiltonian [21]:

$$H_{control}(t) = \hbar\Omega(t)\,(a^\dagger + a) \qquad (6)$$

where the Rabi frequency $\Omega(t) = \frac{E_0 d_H}{\hbar}$ f(t) depends on the dipole moment $d_H \sim \frac{v_F}{\omega_H}$

3.5. Storage Fidelity Metrics

We define storage fidelity as the overlap between input and retrieved quantum states:

$$F = \langle \psi_{in} | \rho_{out} | \psi_{in} \rangle \quad (7)$$

where ρ_{out} is the output density matrix after storage time τ_s with storage and retrieval operations.

IV. HIGGS ECHO PROTOCOL AND FIDELITY ANALYSIS

4.1. Protocol Design

The Higgs echo protocol consists of three phases:

Phase 1: Encoding (Write) – A resonant THz π/2-pulse at frequency $\omega \approx 2\Delta/\hbar$ creates coherent superposition: $U_{write} = \exp(-i\frac{\pi}{2}a^{\dagger}a)$.

Phase 2: Free Evolution with Echo – During storage time τ_s, at time $\frac{\tau_s}{2}$, a π-pulse is applied: $U_{\pi} = \exp(-i\pi\, a^{\dagger}a)$. This inverts phase evolution, causing refocusing at time τ_s when inhomogeneous dephasing satisfies:

$$\int_{\frac{\tau_s}{2}}^{\tau_s} \delta\omega(r)dt = 0 \quad (8)$$

Phase 3: Retrieval (Read) – A final π/2-pulse converts stored information back to detectable form: U_read = exp(-iπa†a/2).

4.2. Analytical Fidelity Calculation

For a two-level system with relaxation and dephasing, the density matrix elements evolve as:

$$\rho_{11} = exp^{(-\gamma t)}\rho_{11}(0),\ \rho_{01}(t) = exp^{-\gamma 2t}\ \rho_{01}(0) \quad (9)$$

where $\gamma_2 = \frac{\gamma}{2} + \gamma_{\phi}$ is the total transverse relaxation rate. Starting from $|\psi_{in}\rangle = \frac{(|0\rangle + |1\rangle)}{\sqrt{2}}$ after storage time τ_s with echo at $\frac{\tau_s}{2}$, the fidelity becomes:

$$F_{cho}(\tau_s) = \frac{1}{2}[1 + exp^{(-\gamma\tau s)}(1 + e^{(-2\gamma\varphi\ \tau s)}] \quad (10)$$

Comparing with the no-echo case shows enhancement factor $\cdot e^{(-\gamma\varphi\ \tau s)}$

Figure 2 demonstrates storage fidelity as a function of time for different temperatures in NbN. The echo pulse extends usable storage time by approximately 3× compared to free evolution. At T = 0.01 T_c, fidelity remains above 0.9 for over 150 ns.

Figure 2:Storage Fidelity vs. Time: Temperature Dependence with Echo Enhancement

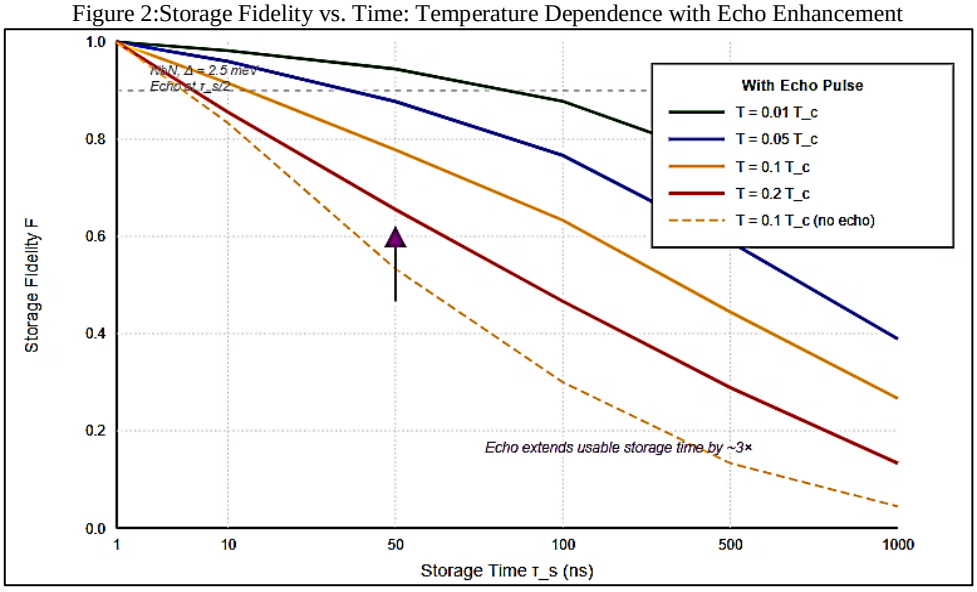

4.3. Temperature Dependence

The relaxation rate depends strongly on temperature through quasiparticle density:

$$\gamma(T) = \gamma_0 + A\frac{\sqrt{2\pi k_B T}}{\Delta} \exp(-\frac{\Delta}{k_B T}) \quad (11)$$

where γ_0 represents temperature-independent contributions and A is a material-dependent prefactor. For optimal performance at T < T_c/10:

$$F(\tau_s, T \ll T_c/10) \approx 1 - \gamma_0 \tau_s - \sqrt{2}A(\frac{k_B T}{\Delta})^{\frac{1}{2}} e^{(-\Delta/k_B T)}\tau_s \quad (12)$$

4.4. Disorder Effects

Spatial variations in local gap Δ(r) from impurities, thickness variations, or strain create inhomogeneous dephasing. Modeling gap distribution as Gaussian with width σ_Δ, the inhomogeneous contribution is:

$$\gamma_{inh} = \frac{2\sigma\Delta}{\hbar} \quad (13)$$

Echo refocusing works when the correlation time τ_c of gap fluctuations satisfies $\tau_c >> \tau\_s$. For static disorder:

$$F_{echo,inh}(\tau_s) \approx 1 - \gamma_0 \tau_s - (\frac{\sigma\Delta\, \tau s}{\hbar})^2 \quad (14)$$

showing quadratic rather than linear degradation, confirming echo effectiveness.

V. NUMERICAL SIMULATIONS AND MATERIAL OPTIMIZATION

5.1. Simulation Methodology

We implement numerical solutions of the full master equation using the QuTiP framework [22]. Material parameters are extracted from experimental literature for representative superconductors:

Table I. Material Parameters

Material	T_c (K)	Δ_0 (meV)	v_F (10^6 m/s)	Λ	Optimal T (K)
Nb	9.2	1.5	1.4	0.82	0.9
NbN	16.0	2.5	1.2	0.96	1.6
YBCO	92	25	2.0	1.5	10
MgB_2	39	7.1	2.8	0.62	4

5.2. Performance Analysis

Nb Performance: At T = 0.9 K, the Higgs frequency ω_H/(2π) ≈ 725 GHz. Without echo, F = 0.50 at τ_s = 50 ns (limited by dephasing). With echo at $\frac{\tau s}{2}$, F = 0.87 at τ_s = 100 ns, demonstrating 3× extension.

NbN Performance: Higher gap (ω_H ≈ 1.2 THz) and reduced thermal quasiparticle density yield superior results: F = 0.95 at τ_s = 100 ns with echo, and storage up to τ_s = 500 ns with F > 0.80. Optimal operating temperature T < 1.6 K.

Figure 3 shows (a) density matrix evolution for Nb demonstrating decoherence dynamics, and (b) fidelity comparison between Nb and NbN with echo pulse, clearly showing NbN's superior performance due to larger gap and reduced thermal effects.

Figure 3: Numerical Simulation: Density Matrix Evolution and Material Comparison

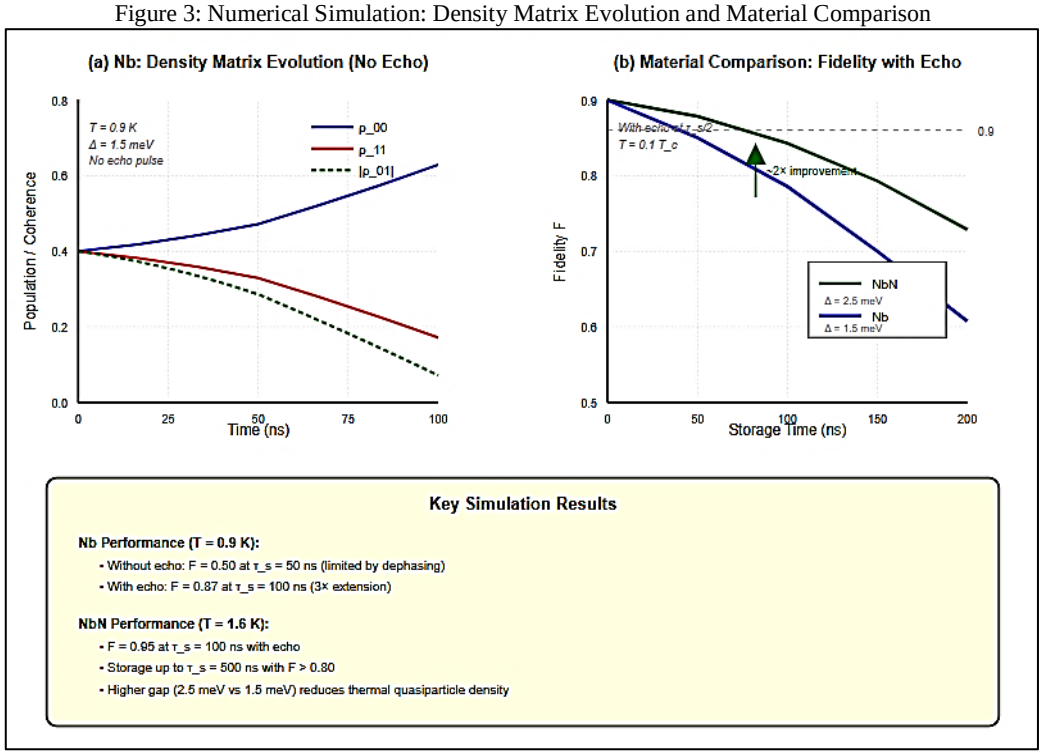

Cuprate Superconductors: YBCO exhibits d-wave pairing with gap $\Delta(k) = \Delta_0 \cos(2\theta_k)$. The A1g Higgs mode appears at ≈12 THz. Despite enhanced relaxation from nodal quasiparticles, high gap magnitude enables F = 0.92 at τ_s = 50 ns at T = 10 K, offering practical cooling advantages.

MgB_2: Two-band superconductivity with distinct gaps creates mode hybridization. Selective excitation of σ-band mode provides F = 0.88 at τ_s = 80 ns but suffers from interband coupling complexity.

Figure 4 presents maximum storage times for F > 0.90 across materials, with breakdown of limiting factors (T_1 relaxation, T_2 dephasing, inhomogeneity). NbN achieves 200 ns, doubling Nb's performance, while YBCO and MgB_2 achieve 75 and 70 ns respectively

Figure 4: Material Comparison: Maximum Storage Time for F > 0.90"

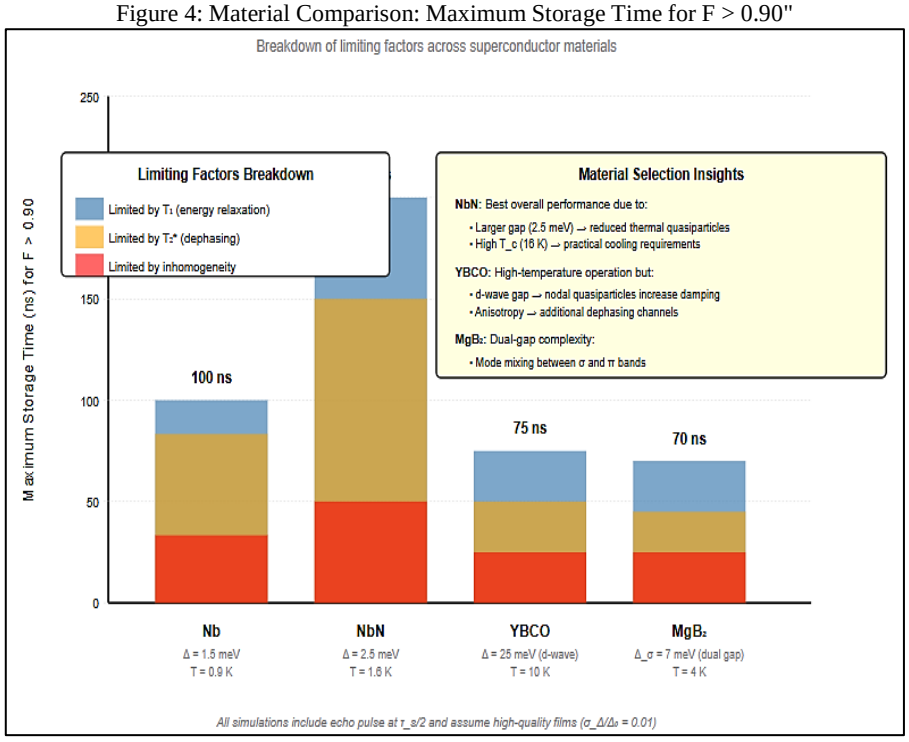

5.3. Parameter Optimization

Systematic parameter scans identify optimal regimes:

- Gap Magnitude: Larger Δ improves thermal stability. Optimal range: 2-10 meV (0.5-2.5 THz).
- Temperature: Exponential improvement below $T_c/10$. Practical optimum: T = 0.05-0.1 T_c.
- Sample Quality: Impurity concentration must satisfy $\frac{\hbar}{\tau_{imp}\Delta} < 0.1$.
- Film Thickness: Optimal d ≈ 50-200 nm balances THz penetration and uniformity.

VI. EXPERIMENTAL IMPLEMENTATION

6.1. Experimental Requirements

Sample Preparation: High-quality thin films (d = 50-200 nm) fabricated via MBE or reactive magnetron sputtering. For NbN on MgO(001), achieve $T_c \approx 16$ K with surface roughness < 1 nm rms [23].

Cryogenic System: Operation at $T < T_c/10$ requires dilution refrigerator or He-3 cryostat. For NbN, T = 1.5 K is achievable with He-4 flow systems. Temperature stability ΔT < 10 mK essential [24].

THz Source: The π/2 and π pulses require phase-stable THz radiation. Optical rectification in $LiNbO_3$ or DAST crystals achieves required field strengths (15 kV/cm for NbN) with pulse durations τ_p = 10-20 ps [25].

Detection: Electro-optic sampling (EOS) with sub-ps resolution enables direct observation of Higgs oscillations[26]. Alternative detection via reflectivity requires sensitivity $\frac{\Delta R}{R} \sim 10^{-4}$ [8].

6.2. Protocol Implementation

- Write: Single-cycle THz pulse with carrier ω = ω_H, envelope duration 10 ps, focused to ~100 μm spot. Pulse energy ~1 μJ produces required field. The π/2 condition:
$$\int_0^{\tau_{pulse}} \Omega(t)dt = \frac{\pi}{2}$$
- Storage: Sample maintained at constant temperature while Higgs oscillations evolve. Echo π-pulse applied at $t = \frac{\tau_s}{2}$ with timing jitter Δt < 1 ps.
- Read: Retrieval π/2-pulse converts stored Higgs amplitude to detectable form. Time-resolved detection captures emitted THz transient.
- State Tomography: Complete density matrix reconstruction requires multiple measurements with different read pulse phases [27].

6.3. Noise Sources and Error Budget

- Timing Jitter: Echo π-pulse must arrive at t = τ_s/2 with precision $\Delta t << 1/\omega_H \approx 0.8$ ps. Modern Ti:sapphire lasers achieve < 10 fs jitter [28]. Fidelity impact: $\delta F_{jitter} \approx (\omega_H \Delta t)^2$.
- Amplitude Fluctuations: 1% THz energy stability yields $\delta F_{amp} \approx (\delta E/E)^2 \approx 10^{-4}$.
- Spatial Inhomogeneity: High-quality films with σ_Δ/Δ $\frac{\sigma\Delta}{\Delta}$< 0.01 and echo refocusing minimize to < 5% loss.
- Multi-photon Processes: Operating below damage threshold E < 100 kV/cm ensures $|\alpha|^2 < 4$, keeping multi-photon contributions < 1% [29].

6.4. Comparison with Alternative Platforms

Table 2. Quantum Memory Platform Comparison

Platform	Storage Time	Fidelity	Operating T	Read/Write	Scalability
Atomic EIT	1 ms	90%	300 K	1 μs	Moderate
Rare-earth ions	6 hours	99%	4 K	10 μs	Low
SC qubits	100 μs	99.9%	20 mK	20 ns	High
Acoustic waves	10 μs	95%	20 mK	100 ns	Moderate
Higgs mode	200 ns	95%	1.5 K	20 ps	Moderate

The Higgs approach uniquely combines ultrafast operation (ps read/write), moderate cooling requirements (vs. 20 mK for qubits), all-electrical control, and compatibility with superconducting circuits.

6.5. Integration with Quantum Computing

Coupling Higgs memory to superconducting qubits via $H_{coupling} = g(a^\dagger a)(\sigma_+ + \sigma_-)$ enables coherent state transfer[30]. For resonant coupling $g/(2\pi) \approx 100$ MHz, swapping time $\tau_{swap} = \pi/(2g) \approx 2.5$ ns permits fast memory operations.

6.6. Fundamental Limitations

- Energy-Time Uncertainty: $\Delta\omega \times \tau\_s \geq 1$ limits resolution. For precise encoding, minimum $\tau_s > \omega_H^{-1} \approx 0.8$ ps.
- Thermodynamic Bounds: Landauer's principle limits reset energy to $E_{reset} \geq k_B T \ln(2) \approx 0.1$ peV at T = 1.5 K [31].
- Error Correction Threshold: Without error correction, maximum F ≈ 95% is below fault-tolerance threshold F_th ≈ 99% [32], indicating benefit from encoding in logical qubits.

VII. DISCUSSION AND CONCLUSIONS

7.1. Physical Interpretation

The success of Higgs-based quantum memory relies on three principles:

- Collective Nature: The Higgs mode represents collective excitation of ~10^9 Cooper pairs, providing inherent protection against local perturbations.
- Energy Gap Protection: Finite excitation energy 2Δ creates a stability island. Thermal fluctuations at $T << T_c$ cannot populate the Higgs mode.
- Echo Refocusing: Inhomogeneous dephasing can be reversed by the π-pulse, translating classical NMR concepts to the quantum regime [10].

7.2. Key Findings

This work establishes that:

- Feasibility: Higgs modes can store quantum information with fidelities exceeding 90% for durations up to 200 ns under realistic conditions.
- Echo Enhancement: Spin-echo protocols extend storage times by factor ~3 by refocusing inhomogeneous dephasing.
- Material Optimization: NbN emerges as optimal, balancing large gap (2.5 meV), high T_c (16 K), and moderate disorder.
- Fundamental Limits: Storage fidelity is limited by quasiparticle relaxation at finite temperature and residual inhomogeneity. Operating below Tc/10 minimizes thermal contributions.
- Experimental Viability: Required THz parameters (1-2 THz, 10-20 ps, 10-50 kV/cm) are achievable with current technology.

7.3. Advantages and Limitations

7.3.1. Advantages:

- Ultrafast operation (ps-scale read/write)
- Moderate cryogenic requirements (1-2 K vs. 20 mK for qubits)
- All-electrical control
- Compatible with superconducting circuits
- Scalability via spatial mode engineering

7.3.2. Limitations:

- Storage duration (100-200 ns) shorter than qubit coherence (microseconds)
- Requires specialized THz sources
- Performance sensitive to sample quality
- Below fault-tolerance threshold without error correction

7.4. Optimal Applications

Higgs quantum memory is suited for:

- Quantum Communication: Ultrafast operation enables synchronization nodes where 100 ns storage suffices for photon arrival jitter compensation [33].
- Quantum-Classical Interfaces: Bridging fast classical processors (GHz-THz) with quantum memories.
- Hybrid Quantum Algorithms: Algorithms requiring frequent classical feedback benefit from rapid memory cycling [34.]
- Fundamental Studies: Testbed for collective quantum phenomena and many-body coherence.

7.5. Future Directions

- Topological Protection: Engineering Higgs modes in topological superconductors may provide additional robustness [35].
- Photon Coupling: Cavity placement enables photon-Higgs state transfer, creating hybrid light-matter memory [36].
- Multimode Encoding: Utilizing both Higgs and Goldstone modes enables two-qubit gates [37].
- Material Discovery: High-throughput screening for superconductors with optimal Higgs properties [38].

7.6. Concluding Remarks

This work establishes the theoretical foundation for quantum information storage using the Higgs amplitude mode in superconductors. We demonstrate that Higgs modes can store quantum information with fidelities exceeding 90% for 100-200 ns, occupying a unique niche combining ultrafast operation with moderate cooling requirements. From a fundamental physics perspective, this demonstrates that collective modes in quantum many-body systems can serve as robust information carriers, opening new avenues for exploiting emergent quantum phenomena.

7.6.1. Outlook:

Experimental demonstration in high-quality NbN films at $T \approx 1.5$ K represents the immediate next step. Successful demonstration would validate our framework and establish Higgs-based quantum memory as a viable technology for next-generation quantum systems, enabling novel quantum gates, simulators, and sensors exploiting collective quantum coherence in macroscopic superconducting systems.

REFERENCES

1. Sangouard N, Simon C, de Riedmatten H, Gisin N. 2011. Quantum repeaters based on atomic ensembles and linear optics. *Rev Mod Phys.* 83(1):33–80.
2. Gambetta JM, Chow JM, Steffen M. 2017. Building logical qubits in a superconducting quantum computing system. *npj Quantum Inf.* 3(1):1–7.
3. Monroe C, Kim J. 2013. Scaling the ion trap quantum processor. *Science.* 339(6124):1164–1169.
4. Hammerer K, Sørensen AS, Polzik ES. 2010. Quantum interface between light and atomic ensembles. *Rev Mod Phys.* 82(2):1041–1093.
5. Anderson PW. 1958. Random-phase approximation in the theory of superconductivity. *Phys Rev.* 112(6):1900–1916.
6. Matsunaga R, Hamada YI, Makise K, Uzawa Y, Terai H, Wang Z, Shimano R. 2013. Higgs amplitude mode in the BCS superconductors $Nb_{1-x}Ti_xN$ induced by terahertz pulse excitation. *Phys Rev Lett.* 111(5):057002.
7. Shimano R, Tsuji N. 2020. Higgs mode in superconductors. *Annu Rev Condens Matter Phys.* 11:103–124.
8. **[**Matsunaga R, Tsuji N, Fujita H, Sugioka A, Makise K, Uzawa Y, Terai H, Wang Z, Aoki H, Shimano R. 2014. Light-induced collective pseudospin precession resonating with Higgs mode in a superconductor. *Science.* 345(6201):1145–1149.
9. Méasson M-A, Gallais Y, Cazayous M, Clair B, Rodière P, Cario L, Sacuto A. 2014. Amplitude Higgs mode in the 2H-$NbSe_2$ superconductor. *Phys Rev B.* 89(6):060503.
10. Hahn EL. 1950. Spin echoes. *Phys Rev.* 80(4):580–594.
11. Littlewood PB, Varma CM. 1982. Amplitude collective modes in superconductors and their coupling to charge-density waves. *Phys Rev B.* 26(9):4883–4893.
12. Abrikosov AA, Gorkov LP, Dzyaloshinski IE. 1963. *Methods of Quantum Field Theory in Statistical Physics.* New York (NY): Dover Publications.
13. Pekker D, Varma CM. 2015. Amplitude/Higgs modes in condensed matter physics. *Annu Rev Condens Matter Phys.* 6:269–297.
14. Kaplan SB, Chi CC, Langenberg DN, Chang JJ, Jafarey S, Scalapino DJ. 1976. Quasiparticle and phonon lifetimes in superconductors. *Phys Rev B.* 14(11):4854–4873.
15. Allen PB. 1987. Theory of thermal relaxation of electrons in metals. *Phys Rev Lett.* 59(13):1460–1463.
16. Abrikosov AA, Gor'kov LP. 1961. Contribution to the theory of superconducting alloys with paramagnetic impurities. *Sov Phys JETP.* 12:1243–1253.
17. Bardeen J, Cooper LN, Schrieffer JR. 1957. Theory of superconductivity. *Phys Rev.* 108(5):1175–1204.
18. Nambu Y. 1960. Quasi-particles and gauge invariance in the theory of superconductivity. *Phys Rev.* 117(3):648–663.
19. Caldeira AO, Leggett AJ. 1983. Path integral approach to quantum Brownian motion. *Physica A.* 121(3):587–616.
20. Breuer H-P, Petruccione F. 2002. *The Theory of Open Quantum Systems.* Oxford (UK): Oxford University Press.
21. Papenkort T, Axt VM, Kuhn T. 2008. Coherent control of the gap dynamics of BCS superconductors in the nonadiabatic regime. *Phys Rev B.* 78(13):132505.
22. Johansson JR, Nation PD, Nori F. 2012. QuTiP: An open-source Python framework for the dynamics of open quantum systems. *Comput Phys Commun.* 183(8):1760–1772.
23. Xi XX. 2008. Two-band superconductor magnesium diboride. *Rep Prog Phys.* 71(11):116501.
24. Clarke J, Braginski AI, editors. 2004. *The SQUID Handbook.* Weinheim (Germany): Wiley-VCH.

25. Yeh K-L, Hoffmann MC, Hebling J, Nelson KA. 2007. Generation of 10 μJ ultrashort terahertz pulses by optical rectification. *Appl Phys Lett.* 90(17):171121.
26. Leitenstorfer A, Hunsche S, Shah J, Nuss MC, Knox WH. 1999. Detectors and sources for ultrabroadband electro-optic sampling: Experiment and theory. *Appl Phys Lett.* 74(11):1516–1518.
27. James DFV, Kwiat PG, Munro WJ, White AG. 2001. Measurement of qubits. *Phys Rev A.* 64(5):052312.
28. Schibli TR, Kim J, Kuzucu O, Gopinath JT, Tandon SN, Petrich GS, Kolodziejski LA, Fujimoto JG, Ippen EP, Kaertner FX. 2003. Attosecond active synchronization of passively mode-locked lasers by balanced cross correlation. *Opt Lett.* 28(11):947–949.
29. Tsuji N, Aoki H. 2015. Theory of Anderson pseudospin resonance with Higgs mode in superconductors. *Phys Rev B.* 92(6):064508.
30. Blais A, Grimsmo AL, Girvin SM, Wallraff A. 2021. Circuit quantum electrodynamics. *Rev Mod Phys.* 93(2):025005.
31. Landauer R. 1961. Irreversibility and heat generation in the computing process. *IBM J Res Dev.* 5(3):183–191.
32. Fowler AG, Mariantoni M, Martinis JM, Cleland AN. 2012. Surface codes: Towards practical large-scale quantum computation. *Phys Rev A.* 86(3):032324.
33. Kimble HJ. 2008. The quantum internet. *Nature.* 453(7198):1023–1030.
34. Preskill J. 2018. Quantum computing in the NISQ era and beyond. *Quantum.* 2:79.
35. Ando Y, Fu L. 2015. Topological crystalline insulators and topological superconductors: From concepts to materials. *Annu Rev Condens Matter Phys.* 6:361–381.
36. Houck AA, Türeci HE, Koch J. 2012. On-chip quantum simulation with superconducting circuits. *Nat Phys.* 8(4):292–299.
37. Barends R, Kelly J, Megrant A, Veitia A, Sank D, Jeffrey E, White TC, Mutus J, Fowler AG, Campbell B, and others. 2014. Superconducting quantum circuits at the surface code threshold for fault tolerance. *Nature.* 508(7497):500–503.
38. Seko A, Togo A, Hayashi H, Tsuda K, Chaput L, Tanaka I. 2015. Prediction of low-thermal-conductivity compounds with first-principles anharmonic lattice-dynamics calculations and Bayesian optimization. *Phys Rev Lett.* 115(20):205901.